Impact of damping boundaries on the quality of the output signal in bender element experiments

Mohammad Jawed Roshan[1], *Daniela* Bendea[2,3], *Ionut Dragos* Moldovan[2,3#], *Marcos* Martins[4], *Monika Grazyna* Pultorak[1], *António Gomes* Correia[1], and *Miguel* Azenha[1]

[1]*Department of Civil Engineering, ISISE, University of Minho, Campus de Azurém, 4800-058 Guimarães, Portugal*
[2]*CERIS, Instituto Superior Técnico, Universidade de Lisboa, Av . Rovisco Pais, 1049-001, Lisboa, Portugal*
[3]*Engineering Department, Lusófona University, Campo Grande, 1700-097, Lisboa, Portugal*
[4] *INESC TEC, R. Dr. Roberto Frias, 4200-465 Porto, Portugal*
[#]*Corresponding author: dragos.moldovan@ulusofona.pt*

ABSTRACT

Bender elements are a popular experimental device for the measurement of the small strain shear modulus of geomaterials. Bender elements are easy to use, can be easily installed in most geotechnical devices (e.g., triaxial apparatus, oedometers, and Rowe cells), and yield shear modulus readings that compare well with those obtained from resonant column tests.
Typically, bender element tests involve inducing a shear wave at one end of a sample (the input signal) and reading its arrival at the other end (the output signal). However, the wave propagation induced by bender elements is complex, hindering the interpretation of the output signal and inducing considerable uncertainty in the shear modulus readings. Indeed, besides the desirable shear wave, the vibration of the transmitter also generates laterally propagating compression waves, which reflect from the lateral envelope back into the sample and pollute the output signal.
This study analyses the effect of lateral boundaries especially conceived to dampen the incoming compression waves on the quality of the output signal. In this context, damping moulds are designed based on computational simulations of the transient dynamics of the wave propagation, to promote an output signal that presents a clearly identifiable arrival of the shear wave, without it being concealed by compression wave pollution. Prototypes of a few promising designs are produced using 3D printing and tested in the laboratory using a benchmark material (Toyoura sand) and a range of input frequencies. The results are compared with those obtained in a conventional setup with no damping moulds.

Keywords: bender element, shear wave, compressive wave, hybrid-Trefftz finite element.

1. Introduction

The small strain shear modulus (G0) is a crucial soil property in various geotechnical applications such as liquefaction assessment, earthquake ground response analysis, evaluation of road and railway track, behaviour of structures subjected to cars and train induced vibrations, and design of foundations under dynamic loading. The small strain shear modulus can be computed from the velocity of the shear (S) waves (Cai et al. 2015; Lings and Greening 2001), using various techniques, including dynamic testing with resonant column or bender elements (BEs), and quasi-static loading test with high-resolution strain measurements (Gu et al. 2015). However, BE testing is cheaper, more adaptable to other geotechnical devices (e.g., triaxial, oedometer, and Rowe cell), and easier to use. For these reasons, the piezoceramic BE are widely used in geotechnical engineering (Ingale, Patel, and Mandal 2017).

Although the shear velocity can be readily obtained by measuring the travel time of the shear wave between the transmitter and receiver, there are many uncertainties, caused by wave interferences at the rigid boundary and wave absorption by equipment walls, which leads to the pollution of the shear wave with secondary compression (P) waves (Moldovan, Correia, and Pereira 2016). Open scientific debate also exists on the optimal specimen geometry and location of the receiver BE (Moldovan and Correia 2021).

The reliability of shear modulus calculation resulting from measured shear wave velocity depends on all factors mentioned above. To date, some studies have been conducted to enhance the quality of the output signal (Ingale, Patel, and Mandal 2020; Liu et al. 2022; Moldovan and Correia 2017). For instance, to improve the reliability of the measured arrival time of the shear wave and to differentiate between shear and compression waves, Moldovan and Correia (2021) investigated the best and most suitable location of receiver BE based on computational analysis. According to their results, the geomaterial and testing conditions affect the optimal location of the receiver BE, indicating that the optimal position of the receiver BE is a problem-dependent issue.

Besides optimizing the location of receiver BE, an alternative option is to dampen the P-wave reflected from the geomaterial envelope. However, to the best of the authors' knowledge, this issue has not yet been covered in previous studies. Thus, it needs to be investigated based on numerical modelling and experimental testing. Therefore, this paper reports on an attempt to change the geometry of the side walls of the recipient containing the

soil sample in order to dampen the inbound compression waves, ideally resulting in increased reliability of the BE test. First, numerical modelling was conducted using the hybrid-Trefftz finite element platform FreeHyTE (Moldovan et al. 2021) (Cismasiu et al. 2017; Moldovan et al. 2021); then, based on the numerical findings, a few promising wall designs were produced by 3D printing and used in BE tests to observe their effects.

2. Numerical assessment

The estimation of the travel time of the shear wave between the transmitter and receiver BE is typically done using time-domain and frequency domain methods. However, there is no universally accepted procedure because of the issues affecting the output signals (Ogino 2019). In order to increase the reliability of BE tests, numerical analysis has been performed by previous researchers, mostly using the finite element method (Ingale et al. 2020; Jovičić, Coop, and Simić 1996; Rahman et al. 2016) and discrete element method (O'Donovan, O'Sullivan, and Marketos 2012). However, the numerical analysis typically requires small time steps and refined meshes to achieve convergence and reliable results. For instance, Jovičić et al. (Jovičić et al. 1996) applied 2000 elements and a small time-step in SOLVIA 90 package to model the BE test of white kaolin soil. Liu et al. (Liu et al. 2021) modelled the BE testing of Ottawa sand specimens with height and width of 140 mm and 70 mm, respectively, using COMSOL software. The specimens were discretized with 5145 elements. In a parametric study, Ingale et al. (Ingale et al. 2020) suggested that the leading size of a finite element in an ABAQUS model be one twentieth of the wavelength to achieve a smooth waveform. In numerical modeling, the reliability and precision of the outputs decrease with the increase in meshing dimensions (i.e., the larger the meshing, the lower the precision of outputs) (Rahman et al. 2016).

To overcome such limitations, in a recent study (Moldovan, Correia and Pereira 2016), hybrid-Trefftz finite elements were used to model BE experiments. Hybrid-Trefftz elements are much less sensitive than conventional finite elements to short wavelengths (Moldovan et al. 2021), enabling the modelling of multi-phase materials, including the elusive compression waves propagating through the fluid phases. Moreover, due to their physically meaningful approximation bases, hybrid-Trefftz elements can efficiently filter the polluting compression waves out of the output signals, resulting in a more reliable measuring of the small strain shear modulus (Moldovan, Correia and Pereira 2016). The hybrid-Trefftz finite element platform FreeHyTE (Moldovan and Cismaşiu 2018) was used to construct the models. FreeHyTE is an open-source and user-friendly software that can simulate solid (single-phase), fully saturated (biphasic) and unsaturated (triphasic) geomaterials (Climent, Moldovan, and Correia 2022). It was successfully employed to simulate the response of geomaterials under highly transient loading (Moldovan et al. 2021).

In the current study, the FreeHyTE platform is employed to model the wave propagation through a sample of Toyoura sand confined in the relatively tall cylinder shown in Fig. 1.

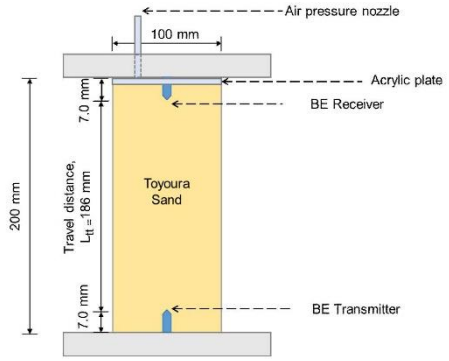

Figure 1. Bender element setup.

As thoroughly shown in previous studies (Moldovan, Correia and Pereira 2016), the output signal tends to be heavily polluted with compression waves when the height of the sample is larger than its width. This happens because of the propagation patterns of the waves triggered by the lateral vibration of the transmitter, as illustrated in Fig. 2. Indeed, the vibration of the transmitter induces not only a vertically propagating shear wave, but also a pair of compression waves that propagate laterally, towards the vertical enclosure of the sample. Because of the impedance difference between the sample and the lateral walls, a part of the energy contained in these compression waves reflects towards the centre of the sample, affecting the readings of the receiver.

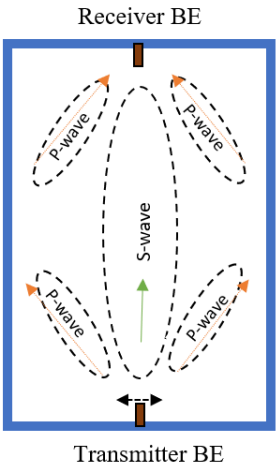

Figure 2. S- and P-wave propagation in the original recipient.

To hinder the reflection of the compression waves from the lateral walls, an obvious solution is to substitute them with a lateral boundary designed to dampen the reflections (Fig. 3). The damping boundary is profiled with spikes that scatter the incoming waves instead of allowing them to reflect them as a compact wave pack. The spikes need to be as less invasive as possible, in order to avoid the perturbation of the geomaterial, but large enough to achieve their desired effect. Two dimensions are essayed, namely 3 mm protrusion height with an 8 mm base (3x8 mm), and 7 mm protrusion height with a 15 mm base (7x15 mm). In both cases the flat space between consecutive spikes is 5 mm.

The effect of the presence of the spikes on the quality of the output signal was analysed using the biphasic hybrid-Trefftz model implemented in FreeHyTE. The models assume that the geomaterial is subjected to plane strain conditions. This assumption is indeed not exceedingly realistic, but plane strain models have been proved to yield output signals qualitatively similar to those obtained in the lab (Moldovan, Correia and Pereira 2016) and are therefore deemed sufficient for the current purpose.

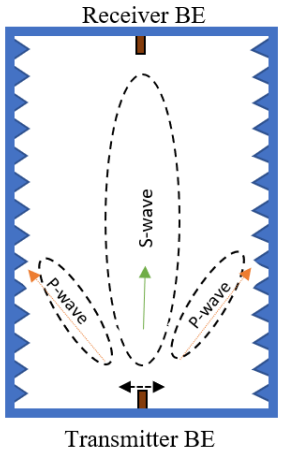

Figure 3. S- and P-wave propagation in the recipient with damping boundaries.

The discretization of these models is made using triangular finite elements and their mesh refinement is presented in Fig. 4. The BE setup with flat walls (Fig. 4(a)) presents a coarse mesh, formed of only 710 finite elements. The model with the damping walls with spikes of 3x8 mm is built using 2761 finite elements, as the size of the elements is constrained by the small dimensions of the spikes (Fig. 4(b)). For the case with larger spikes, the mesh needs not be so fine and is constructed with 693 finite elements (Fig. 4(c)). The input signal is a single sine pulse with a frequency of 2kHz and the vibration amplitude of the transmitter is set to 1 μm.

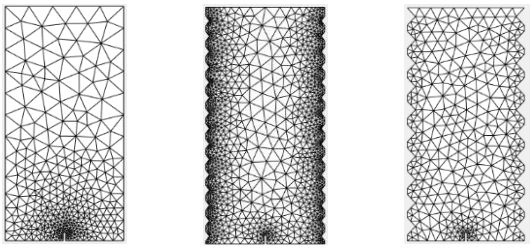

(a) Reference test (b) 3x8 mm spikes (c) 7x15mm spikes

Figure 4. Computational models.

The time-histories of the horizontal displacements at the tip of the receiver for each of the three models are presented in Fig. 5.

For a better illustration of the finite element solution, the horizontal displacement solutions over the whole domain are plotted at the six different instants, indicated in Fig. 6 to Fig. 8.

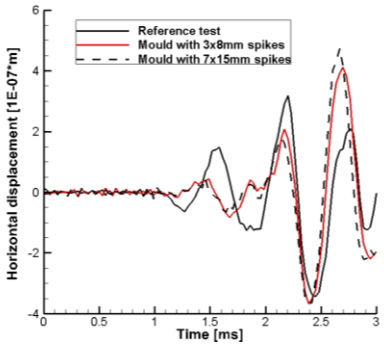

Figure 5. Horizontal displacements at the tip of the receiver.

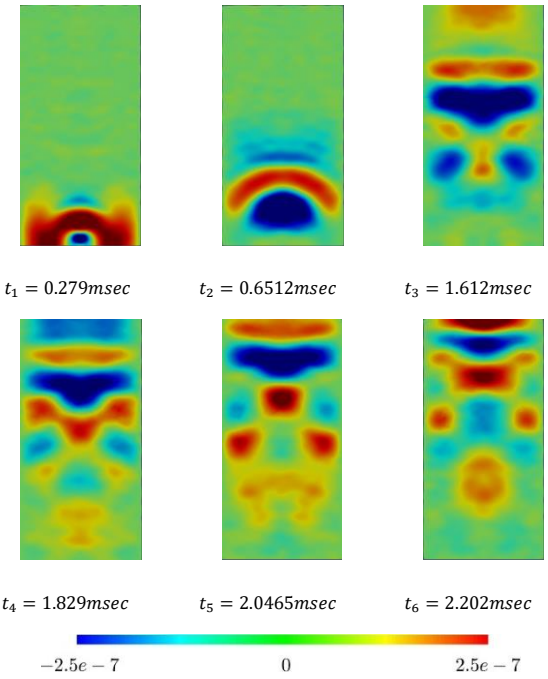

Figure 6. Horizontal displacement fields obtained with the reference test model.

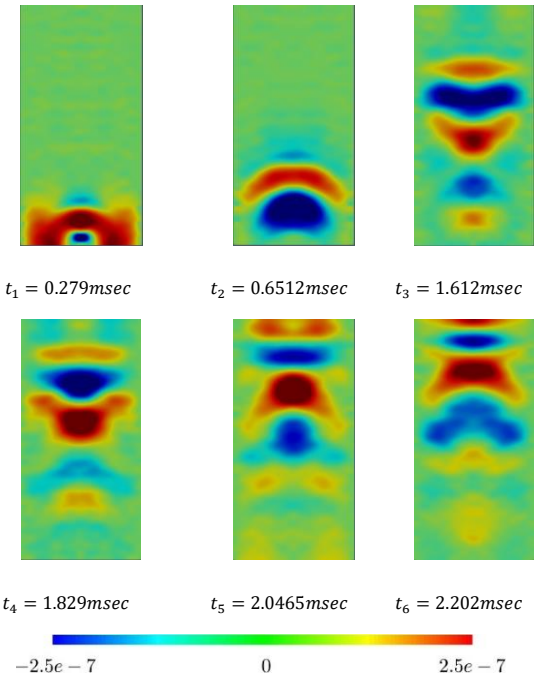

Figure 7. Horizontal displacement fields obtained with the model with 3x8 mm spikes.

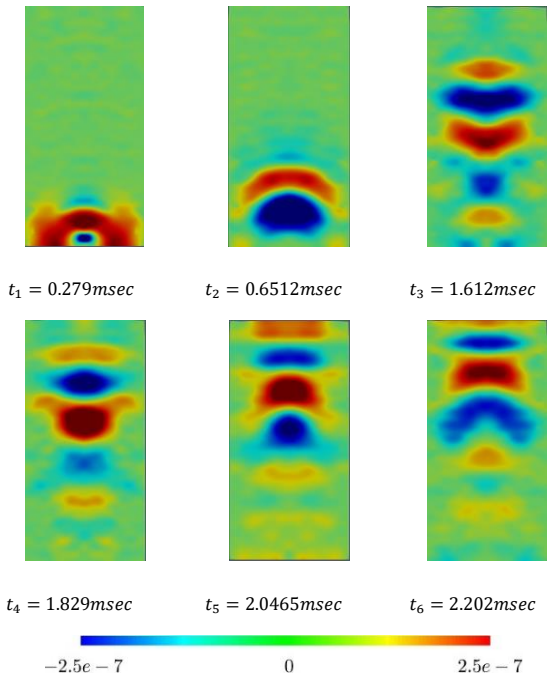

Figure 8. Horizontal displacement fields obtained with the model with 7x15 mm spikes.

The output signal obtained for the reference test in Fig. 5 presents the typical compression wave pollution that tampers with the arrival of the shear wave. Indeed, the signal amplitude occurring around 1.6 ms is caused by the early arrival of the compression waves reflected from the lateral boundary, as seen in the third colour plot in Fig. 6. According to the numerical model, it is only the second amplitude, around 2.1 ms that is the actual arrival of the shear wave, as indicated by the last two colour plots in Fig. 6.

The presence of the lateral spikes, on the other hand, dampens considerably the intensity of the early compression wave, as visible in the time-history plots in Fig. 5. This is particularly obvious in the third colour plots in Fig. 7 and Fig. 8. The intensity of the shear wave also suffers a slight loss in intensity (see the last two plots in Fig. 7 and Fig. 8), but the signal is still strong enough not to pose any problems to the recovery of the shear modulus. The output signals obtained with the two damping boundaries are very similar, no significant benefit having seemingly be obtained with the larger sizes of the spikes. Therefore, the solution with spikes of 3x8 mm were adopted, because their reduced dimensions should be less invasive for the geomaterial.

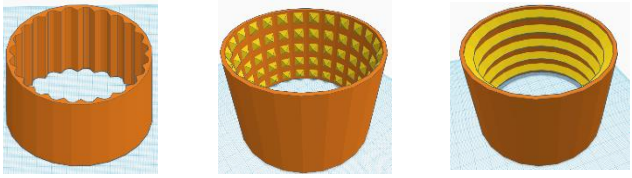

a) Mould w/ strips b) Mould w/ spikes c) Mould w/ rings

Figure 9. Printed prototypes of the mould with 3x8mm spikes.

Three lateral moulds were designed for 3D printing, as presented in Fig. 9. The last two damping moulds present the same cross section in 2D, so they both correspond to the essayed model. The first model was added as it presents the practical advantage of being able to collect a soil sample in the field with minimal disturbance.

The experimental tests for the validation of the numerical findings are described in the next section.

3. Validation

3.1. Material and sample preparation

In the current study, Toyoura sand, a Japanese benchmark geomaterial, was employed to avoid the influence of grain size on the recorded signals. Toyoura sand is classified as a poorly graded clean sand (SP) according to the Unified Soil Classification System. The physical characteristics of the Toyoura sand are tabulated in Table 1.

Table 1. Properties of Toyoura sand

Property	Value
Specific gravity	2.65
Maximum void ratio	0.968
Minimum void ratio	0.628
Maximum dry density (g/cm3)	1.628
Minimum dry density (g/cm3)	0.628
Mean grain size, D50 (mm)	0.15
Coefficient of uniformity	1.43

The soil samples were prepared using the dry tamping method in 5 equal layers with a void ratio e=0.79 (i.e., Dr=52%). After oven-drying the sand overnight, the quantity of sand needed for each layer was precisely weighed and then poured into the mould. Then the top surface of the sand layer was flattened and tamped to the desired level, to achieve homogeneity throughout the sample.

3.2. Bender element setup and testing procedure

In the current study, the BE elements were fabricated by the authors. The transmitter BE at the bottom of the cell and receiver BE at the top cap of the cell are rectangular in shape, with the same size (13 mm width, 7 mm cantilever length and 2.5 mm thickness), as seen in Fig. 10. The active element of the BE consists of a piezoceramic trimorph bending actuator in carbon fiber technique, which allows a maximum deflection of 0.14mm at 230V and a blocking force on each side of 2.3N at 230V. Ancillary devices, such as a signal generator (TTi, Huntingdon TG2511), a digital Oscilloscope, and a personal computer for displaying the Picoscope 6 software, were used to induce and receive signals. Fig. 10 presents an overview of the BE setup.

The damping moulds for the current study were produced using 3D printing technology. The mould design in CAD software was prepared into gcode for 3D printing using the Slicer software. Basic PLA (polyactide) filament was used to print the moulds.

The inner side of the moulds feature the vertical strips, spikes, and rings, as seen in Fig. 11, whose purpose is to dampen the propagation of the compression waves, as discussed in Section 2.

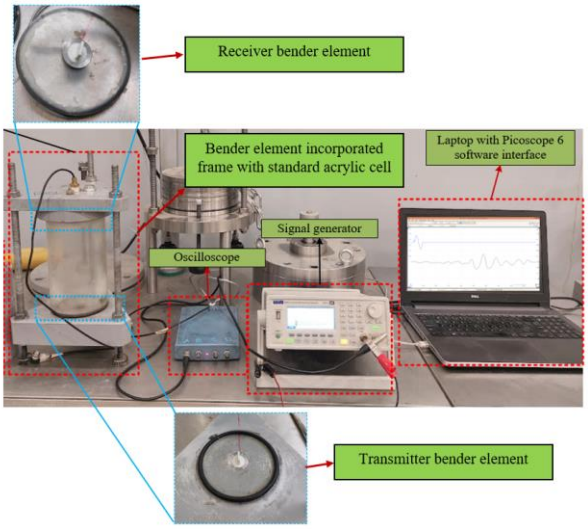

Figure 10. Overview of BE setup

The height and diameter of the standard acrylic cell are 200 mm and 100mm, respectively. However, the 3D printed moulds slightly smaller than 100 mm in diameter to fit inside the standard acrylic cell. To assess the effect of the damping moulds, tests were also carried out using standard acrylic cells (i.e., with a smooth inner surface). After preparing the sand samples with the dry tamping method in 5 layers, the transmitter BE at the bottom of the testing setup was excited by applying sinusoidal pulses with frequencies of 2 kHz, 3.5 kHz, and 4 kHz, and voltage amplitude of 10 V. Then, the output signals were registered by the receiver BE at the top of sample and recorded using the Picoscope 6 software.

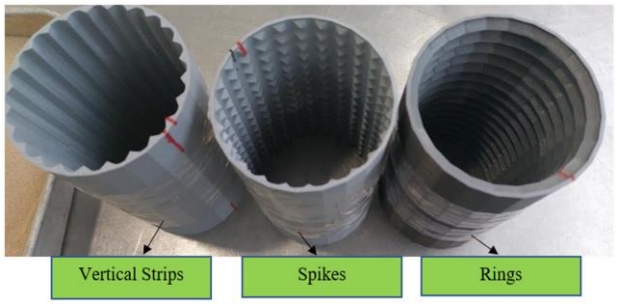

Figure 11. 3D printed moulds

3.3. Results and discussions

Fig. 12 presents the sinusoidal pulse input signal and the time-histories of the output signals for the standard setup with the standard acrylic cell (flat walls) and the three damping moulds, under 2 kHz excitation frequency. As expected, for the standard setup, the output signal is polluted by compression waves reflected from the side walls, which may result in errors when the shear modulus is calculated based on arrival time picking methods[OBJ][OBJ]. Indeed, pinpointing the first arrival looks like a challenging task for the standard acrylic cell, owing to various low amplitude peaks before the prominent ones. Visually, the first arrival in the case of the standard acrylic cell can easily be assumed to be point A or C, let alone the early peak at roughly 1 ms. However, the peak B strongly decreases when the damping moulds are used. A numerical study demonstrated that the early arrival waves before the main peaks are reflected P-wave from boundaries[OBJ][OBJ]. Therefore, it seems that the damping moulds are effective in dissipating the incoming compression waves, resulting in an output signal that enables the clearer identification of the shear wave arrival.

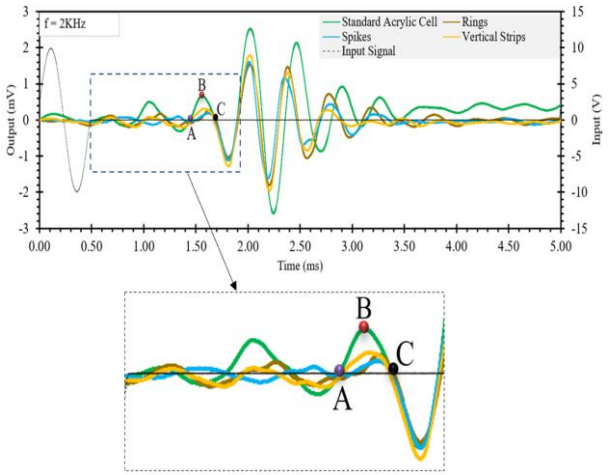

Figure 12. Output signals, f = 2 kHz

Moreover, while all damping moulds seem effective, it is worth noting that the moulds with spikes and ring shapes have more influence in reducing the compressive wave. On the other hand, the vertical strips mould presents the additional advantage of being less disturbing for homogeneity of the specimen.

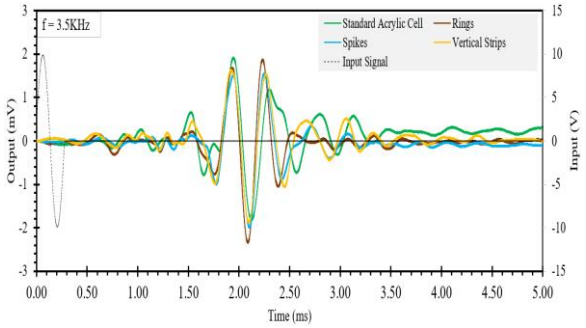

Figure 13. Output signals, f = 3.5 kHz

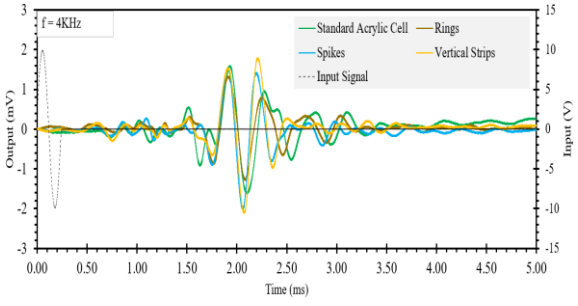

Figure 14. Output signals, f = 4 kHz

Similarly, the output signals for 3.5 kHz and 4 kHz excitation frequency also illustrate the reduction of peak B in the case of 3D printed moulds, as seen in Fig. 13 and Fig. 14. While the experiments reported in this study are rather incipient and additional studies will be needed to assess the effectiveness of the damping moulds under different experimental conditions, it is safe to say that they seem to successfully scatter the incoming compression waves, leading to clearer output signals.

This also clearly raises the importance of boundary conditions in identifying the arrival of shear waves and hence in deducing the small strain shear modulus.

4. Validation

In the current study, we assess the effects of lateral damping boundaries on the attenuation of the compression waves that are known to pollute the output signals in BE experiments. The design of the damping boundaries is established based on the simulation of the BE tests using numerical models based on hybrid-Trefftz finite elements. Hybrid-Trefftz elements are well suited for modelling problems involving the high excitation frequencies and complex, multi-phase materials that typify BE experiments. The numerical models indicate that protruding spikes are probably effective to scatter incoming compression waves, thus preventing them to reach the receiver with enough energy to create an ample output signal. On the other hand, their protruding length is less relevant to their damping ability, so smaller spikes are a better choice, as they are less disturbing for the sample. The damping boundaries have a much smaller damping effect on the propagation of the shear waves, meaning that their use tends to leave the shear wave signal almost intact.

The conclusions of the numerical study are corroborated by lab experiments on a benchmark geomaterial. The use of three 3D-printed damping moulds renders the output signals easier to read and interpret, as the early compression wave signals are dampened out. This is an encouraging result, although further studies will be needed to better understand their strengths and limitations. In particular, the effects of different mould sizes and damping boundaries with different shapes, sizes, and stiffnesses are suggested for future studies.

5. References

Cai, Y., Q. Dong, J. Wang, C. Gu, and C. Xu. 2015. "Measurement of Small Strain Shear Modulus of Clean and Natural Sands in Saturated Condition Using Bender Element Test." Soil Dyn Earthq Eng 76:100–110. http://doi.org/10.1016/j.soildyn.2014.12.013.

Cismasiu, C., A. Pinho Ramos, I. D. Moldovan, D. F. Ferreira, and J. B. Filho. 2017. "Applied Element Method Simulation of Experimental Failure Modes in RC Shear Walls." Comput Concr 19, no. 4:365–374. http://doi.org/10.12989/cac.2017.19.4.365.

Climent, N., I. D. Moldovan, and A. Gomes Correia. "FreeHyTE: A Hybrid-Trefftz Finite Element Platform for Poroelastodynamic Problems." In: Advances in Transportation Geotechnics IV, Lecture Notes in Civil Engineering, Vol. 164, Springer, 2022, pp. 73–86. https://doi.org/10.1007/978-3-030-77230-7_7.

Gu, X., J. Yang, M. Huang, and G. Gao. 2015. "Bender Element Tests in Dry and Saturated Sand: Signal Interpretation and Result Comparison." Soils Found 55, no. 5:951–962. http://doi.org/10.1016/j.sandf.2015.09.002.

Ingale, R., A. Patel, and A. Mandal. 2017. "Performance Analysis of Piezoceramic Elements in Soil: A Review." Sens Actuators A: Phys 262:46–63. http://doi.org/10.1016/j.sna.2017.05.025.

Ingale, R., A. Patel, and A. Mandal. 2020. "Numerical Modelling of Bender Element Test in Soils." Meas: J Int Meas Confed 152:107310. http://doi.org/10.1016/j.measurement.2019.107310.

Jovičić, V., M. R. Coop, and M. Simić. 1996. "Objective Criteria for Determining Gmax from Bender Element Tests." Geotechnique 46, no. 2:357–362. http://doi.org/10.1680/geot.1996.46.2.357.

Lings, M. L., and P. D. Greening. 2001. "A Novel Bender/Extender Element for Soil Testing." Géotechnique 51, no. 8:713–717. http://doi.org/10.1680/geot.2001.51.8.713.

Liu, H., G. Cascante, P. Maghoul, and A. Shalaby. 2022. "Experimental Investigation and Numerical Modeling of Piezoelectric Bender Element Motion and Wave Propagation Analysis in Soils." Can Geotech J 59, no. 3:330-341. http://doi.org/10.1139/cgj-2020-0757.

Moldovan, I. D., and I. Cismaşiu. 2018. "FreeHyTE: A Hybrid-Trefftz Finite Element Platform." Adv Eng Softw 121:98–119. http://doi.org/10.1016/j.advengsoft.2018.03.014.

Moldovan, I. D., N. Climent, E. D. Bendea, I. Cismasiu, and A. Gomes Correia. 2021. "A Hybrid-Trefftz Finite Element Platform for Solid and Porous Elastodynamics." Eng Anal Bound Elem 124:155–173. http://doi.org/10.1016/j.enganabound.2020.12.014.

Moldovan, I. D., and A. Gomes Correia. 2021. "Optimisation of Receiver's Location in Bender Element Experiments Using Computational Wave Filtration." Soil Dyn Earthq Eng 143:106591. http://doi.org/10.1016/j.soildyn.2021.106591.

Moldovan, I. D., A. Gomes Correia, and C. Pereira. 2016. "Bender-Based G0 Measurements: A Coupled Numerical–Experimental Approach." Comp Geo 73:24–36. http://doi.org/10.1016/j.compgeo.2015.11.011.

Moldovan, I. D., and A. Gomes Correia. 2017. "Fixed Point Automatic Interpretation of Bender-Based G0 Measurements." Comp Geo 89:128–142. http://doi.org/10.1016/j.compgeo.2017.04.016.

Moldovan, I. D., and J. A. T. Freitas. 2012. "Hybrid-Trefftz Displacement and Stress Elements for Bounded Poroelasticity Problems." Comp Geo 42:129–144. http://doi.org/10.1016/j.compgeo.2011.12.003.

O'Donovan, J., C. O'Sullivan, and G. Marketos. 2012. "Two-Dimensional Discrete Element Modelling of Bender Element Tests on an Idealised Granular Material." *Granul Matter* 14, no. 6:733–747. http://doi.org/ 10.1007/s10035-012-0373-9.

Ogino, T. 2019. "Travel Time Observation Using Numerical Simulation of Bender Element Testing in Time and Frequency Domain." Soils Found 59, no. 3:657–670. http://doi.org/10.1016/j.sandf.2019.01.001.

Rahman, M. E., V. Pakrashi, S. Banerjee, and T. Orr. 2016. "Suitable Waves for Bender Element Tests: Interpretations, Errors and Modelling Aspects." Period Polytech: Civ Eng 60, no. 2:145–158. https://doi.org/10.3311/PPci.7952.

Acknowledgements

The authors are grateful for the financial support provided by Fundação para a Ciência e a Tecnologia through grants: PTDC/EAM-GTC/29923/2017, 2022.06879.PTDC, 2023.03777.BD, UIDB/04625/ 2020 and UIDB/04029/2020.